Biochimica et Biophysica Acta 1833 (2013) 3314–3325

Contents lists available at ScienceDirect

Biochimica et Biophysica Acta

journal homepage: www.elsevier.com/locate/bbamcr

Mdm10 is an ancient eukaryotic porin co-occurring with the ERMES complex

Nadine Flinner [a], Lars Ellenrieder [b,c], Sebastian B. Stiller [b,c], Thomas Becker [b,d], Enrico Schleiff [a,*], Oliver Mirus [a]

[a] JWGU Frankfurt am Main, Cluster of Excellence Macromolecular Complexes, Centre of Membrane Proteomics, Department of Biosciences, Max-von-Laue Str. 9, 60438 Frankfurt, Germany
[b] Institut für Biochemie und Molekularbiologie, Universität Freiburg, D-79104 Freiburg, Germany
[c] Fakultät für Biologie, Universität Freiburg, D-79104 Freiburg, Germany
[d] BIOSS Centre for Biological Signalling Studies, Universität Freiburg, D-79104 Freiburg, Germany

ARTICLE INFO

Article history:
Received 26 April 2013
Received in revised form 20 September 2013
Accepted 7 October 2013
Available online 14 October 2013

Keywords:
Eukaryotic β-barrel protein
Multiple sequence alignment
Homology modeling
Phylogenetic analysis
ERMES
SAM

ABSTRACT

Mitochondrial β-barrel proteins fulfill central functions in the outer membrane like metabolite exchange catalyzed by the voltage-dependent anion channel (VDAC) and protein biogenesis by the central components of the preprotein translocase of the outer membrane (Tom40) or of the sorting and assembly machinery (Sam50). The mitochondrial division and morphology protein Mdm10 is another essential outer membrane protein with proposed β-barrel fold, which has so far only been found in Fungi. Mdm10 is part of the endoplasmic reticulum mitochondria encounter structure (ERMES), which tethers the ER to mitochondria and associates with the SAM complex. In here, we provide evidence that Mdm10 phylogenetically belongs to the VDAC/Tom40 superfamily. Contrary to Tom40 and VDAC, Mdm10 exposes long loops towards both sides of the membrane. Analyses of single loop deletion mutants of Mdm10 in the yeast *Saccharomyces cerevisiae* reveal that the loops are dispensable for Mdm10 function. Sequences similar to fungal Mdm10 can be found in species from Excavates to Fungi, but neither in Metazoa nor in plants. Strikingly, the presence of Mdm10 coincides with the appearance of the other ERMES components. Mdm10's presence in both unikonts and bikonts indicates an introduction at an early time point in eukaryotic evolution.

1. Introduction

Mitochondria originated from an endosymbiotic event, where an α-proteobacterial ancestor was incorporated by the last common eukaryotic ancestor [1]. During evolution the vast majority of the genetic information was transferred from the symbiont to the host nucleus. Consequently, mitochondria have to take up proteins, lipids and RNAs in order to fulfill the plethora of different biochemical functions in the cell. In addition, transport systems have been established to warrant massive metabolic exchange between the organelle and the cytosol, and mitochondria became a signaling platform for cellular processes like apoptosis. Thus, mitochondria developed from a symbiont to a fully integrated component of the cellular network [2–7].

From their bacterial ancestor mitochondria inherited β-barrel proteins in their outer membrane. One superfamily of β-barrel proteins, for which no direct bacterial predecessor has yet been identified, comprises the so-called 'eukaryotic porins' VDAC and Tom40 [8–12]. Tom40 is the protein-conducting channel of the translocase of the outer membrane (TOM complex) and is essential for cell survival [3,13–16]. The voltage-dependent anion channel (VDAC) mediates exchange of metabolites across the membrane [17,18]. In addition, VDAC was also reported to transport tRNAs [19] and to play a role during apoptosis [20,21]. The NMR and X-ray structures of VDAC revealed that its β-barrel is formed by 19 β-strands [22–24], whereas all so far known bacterial β-barrel proteins are membrane-integrated by an even number of β-strands [25]. Phylogenetic analyses showed that Tom40 is evolutionarily related to VDAC [9,10]. Based on homology modeling using the VDAC structure as a template it was suggested that the β-barrel of Tom40 is formed by 19 β-strands as well, which was recently confirmed by experimental studies of β-barrel folding of Tom40 in yeast mitochondria [9,11,26,27]. Sam50 is an essential β-barrel protein and is the central component of the sorting and assembly machinery (SAM complex), which mediates the folding and insertion of β-barrel precursor proteins into the outer mitochondrial membrane [27–30]. Sam50 belongs to the Omp85 superfamily, which is also present in Gram-negative bacteria and in chloroplasts [31–34]. The fold of the bacterial Omp85 proteins FhaC and BamA was solved by X-ray crystallography and revealed a 16-stranded β-barrel [35,36], which is distinct from the Tom40/VDAC fold.

In Fungi the mitochondrial distribution and morphology protein Mdm10 associates with two protein machineries, which carry out central but different functions in mitochondrial biogenesis [37–40]. Mdm10 binds to the SAM complex [38,41–44], and is part of the endoplasmic reticulum encounter structure (ERMES) [37,39,40].

* Corresponding author. Tel.: +49 69 798 29287; fax: +49 69 798 29286.
E-mail address: schleiff@bio.uni-frankfurt.de (E. Schleiff).

0167-4889/$ – see front matter © 2013 Elsevier B.V. All rights reserved.
http://dx.doi.org/10.1016/j.bbamcr.2013.10.006

Two different views about the function of the Mdm10-containing SAM complex were reported. On the one hand, it was postulated that Mdm10 stimulates the release of β-barrel preproteins from the SAM complex [41]. On the other hand, it was shown that the SAM-Mdm10 complex functions specifically in the assembly of α-helical TOM subunits like Tom22 with Tom40 but not generally in the biogenesis of β-barrel proteins [38,43,44]. Tom7 modulates the assembly of the TOM complex by inducing the dissociation of Mdm10 from the SAM complex [44,45].

The ERMES complex tethers the ER to mitochondria and is composed of Mdm10, Mdm12, Mmm1, Mdm34 and Gem1 [40,46,47]. The tether is most likely required for the transfer of lipids between mitochondria and ER [40,46,48,49]. Consistently, Mdm34, Mdm12 and Mmm1 contain a synaptotagmin-like, mitochondrial and lipid-binding protein (SMP) domain, which belongs to the superfamily of tubular lipid-binding proteins (TULIP) domains [50]. Such domains have been described to bind hydrophobic ligands such as lipids [51]. The individual deletion of ERMES components like Mdm10, Mdm12 and Mmm1 causes in mitochondria an altered lipid content with reduced cardiolipin level, changes of mitochondrial morphology, reduced binding of mitochondria to actin filaments and impaired transport of mitochondria to the budding yeast cell [48,52–57].

The proposed classification of Mdm10 as a β-barrel protein is supported by the presence of a β-signal, the requirement of SAM components for its biogenesis [30,41,58–60] and the suggested phylogenetic relation to 'eukaryotic porins' [8]. However, detailed information on Mdm10 structure and evolution are still missing.

We report that Mdm10 is a member of the eukaryotic porin superfamily. In order to perform a VDAC-guided annotation of secondary structure elements of the highly divergent VDAC, Tom40 and Mdm10 families, we developed a graph-based consensus multiple sequence alignment (MSA) procedure. Based on this consensus MSA we built a homology model of Mdm10 from *Saccharomyces cerevisiae* and by limited proteolysis experiments on isolated mitochondria we test the predicted topology of the protein. Unlike Tom40 or VDAC Mdm10 exposes large loops towards both the cytosol and the intermembrane space. Single deletions of the loop region do not affect Mdm10 functions. Additionally, the MSA was used to analyze conserved properties of the Mdm10 family and to reconstruct a phylogenetic tree of the eukaryotic porin superfamily. We provide evidence that Mdm10 is present in Fungi and also in some early branching groups of unikonts and bikonts and that its appearance is concomitant with the presence of the central ERMES components Mdm12, Mdm34 and Mmm1 reflecting that Mdm10 is a core component of this complex.

2. Material and methods

2.1. Generation of yeast strains and growth conditions

Yeast strains *mdm10*Δ, $MDM10_{HIS}$ and their corresponding wild-type were generated and grown as described [38,44]. To generate the *S. cerevisiae* strains *mdm10ΔL3* (deleted amino acids 84–136), *mdm10ΔL9* (deleted amino acids 216–229), *mdm10ΔL15* (deleted amino acids 317–411) and *mdm10ΔL18* (deleted amino acids 452–481) a plasmid shuffling approach was employed. In the Mdm10 shuffle strain the open reading frame of *MDM10 was disrupted by ADE2 in the presence of pYep352 encoding for wild-type copy of MDM10*. The mutants *mdm10ΔL3*, *mdm10ΔL9*, *mdm10ΔL15* and *mdm10ΔL18* were generated by the quick change approach using pFL39 encoding for *MDM10* and a *TRP1* marker as template. Subsequently, the deletion constructs were transformed into the shuffle strain. Positive clones were selected using the *TRP1* marker of the vector. The wild-type copy of Mdm10 in the pYep352 vector containing the *URA3* marker was lost upon growth on 5-fluoroorotic acid containing medium. The same approach was used to generate Mdm10 loop mutants in the Mmm1ProtA background. The strain expressing ProtA-tagged Mmm1 in the Mdm10 shuffle background was obtained by following the described procedure [39]. For biochemical analysis yeast cells were grown at 30 °C in YPG medium (1% (w/v) yeast extract, 2% (w/v) peptone, 3% (v/v) glycerol). To study the growth serial dilution of cell cultures were spotted on agar plates containing either YPG or YPD (1% (w/v) yeast extract, 2% (w/v) peptone, 2% (w/v) glucose) medium.

2.2. Topology studies in mitochondria

Mitochondria were isolated by differential centrifugation [61]. The protein concentrations of mitochondria were adjusted to 10 mg/ml and aliquoted. Mitochondrial aliquots were shock-frozen in liquid nitrogen and stored at −80 °C until use. For proteinase K treatment mitochondria corresponding to 50 μg protein content were diluted 1:20 in either SEM buffer (250 mM sucrose, 1 mM EDTA, 10 mM MOPS/KOH pH 7.2) or EM buffer (1 mM EDTA, 10 mM MOPS/KOH pH 7.2). Proteinase K was added to a final concentration of 20 μg/ml and incubated for 15 min on ice. To stop the protease activity PMSF was added to a final concentration of 2 mM and the samples were incubated for further 10 min. Subsequently, mitochondria were re-isolated, washed with SEM buffer and lysed under denaturing conditions and subjected to SDS-PAGE. Proteins were detected by Western Blot and by immunodecoration with the indicated antisera.

2.3. In vitro import of radiolabeled precursor proteins, blue native electrophoresis and affinity purifications

Radiolabeled precursor proteins were synthesized in cell-free rabbit reticulocyte lysate (Promega) in the presence of [^{35}S]-methionine. For the import reaction, [^{35}S]-labeled mitochondrial precursor proteins were incubated at 25 °C with isolated mitochondria in import buffer (3% (v/w) BSA, 250 mM sucrose, 80 mM KCl, 5 mM $MgCl_2$, 2 mM KH_2PO_4, 5 mM methionine, 4 mM ATP, 4 mM NADH, 10 mM MOPS/KOH (pH 7.2)). Transfer on ice stopped the import reaction. Mitochondria were re-isolated, washed with SEM buffer and solubilized with digitonin buffer (20 mM Tris/HCl pH 7.4; 50 mM NaCl, 10% (v/v) glycerol, 0.1 mM EDTA) containing 1% (w/v) digitonin for 15 min on ice. Unsoluble material was removed by centrifugation and the import intermediates were separated by blue native gel electrophoresis as described [62]. Affinity purification of the ERMES complex via ProtA-tagged Mmm1 from total cell extract was performed as described [63].

2.4. Identification of eukaryotic porin-like sequences

Sequences of the eukaryotic porin superfamily were collected from the non-redundant (nr) database hosted at NCBI and from several genome projects (Supplementary Table S1) by hmmer (http://hmmer.janelia.org/) using the porin3 pHMM (PF01459), which includes Tom40 and VDAC sequences and the DUF3722 pHMM (PF12519) consisting of Mdm10 sequences from the Pfam database [64]. In order to remove false positive sequences we accepted all significant hits of the HMM search, which do not have other domains according to PfamScan,. A minimal length requirement of 248 amino acids (the 19 β-strands of mmVDAC (PDB: 3EMN) consist of 194 amino acids and for the 18 loops we define a length of 3 each; $194 + 18 * 3 = 248$) was imposed in order to exclude sequence fragments. For the multiple sequence alignment we reduced our dataset to a maximal sequence identity of 70%, which does not affect the alignment drastically [9] with cd-hit [65].

2.5. Identification of ERMES components

Mdm34, Mdm12 and Mmm1 contain a TULIP domain [50]. Because there is no Pfam pHMM available, we have initially collected sequences of all three proteins by BLAST searches with the yeast homologs as input. In the next step we aligned the obtained sequences with MAFFT

v6.847b [66] and generated pHMMs for each protein with hmmer. These three pHMMs were used to search against the nr database and several genome projects (Supplementary Table S1).

Gem1 contains two GTPase domains, which were recognized by the Pfam pHMM Miro (PF08477). We used this pHMM to search against the nr database and several genome projects (Supplementary Table S1) and accepted all sequences, which have two significant hits for this domain.

Both datasets were reduced to a maximal sequence identity of 70% with cd-hit [65]. In order to discriminate the four proteins from other proteins containing a TULIP or GTPase domain, we clustered them with CLANS [67].

2.6. Multiple sequence alignment

In total we calculate m ($m = 1050$) multiple sequence alignments (MSAs) of n sequences with MAFFT v6.847b [66] and screen a large part of the parameter space (substitution matrices: jtt100, jtt150, jtt200, jtt250 and jtt300, op: 1.0–3.0 in 0.1 steps, ep: 0.0–0.9 in 0.1 steps). For each of these m MSAs we extract $n-1$ pair-wise alignments, with sequence a being a member of each pair. Sequence a is the only member of set $A = \{a_1\}$. The other $n-1$ sequences belong to the sequence set $B = \{b_1, b_2, \ldots, b_{n-1}\}$ ($a \notin B$). In contrast to the original sequences the pair-wise alignment contains gaps ('-') and we refer to the pair-wise alignment of sequences a_1 and b_j as a_1' and b_j'. The i^{th} column of this alignment is referred to as $a_1'_i$ and $b_j'_j$. Sequence a_1 is the amino acid sequence of the structural reference (a_1 = mmVDAC) and has the length z. For clarity we have listed all used symbols and indices in Table 1.

The steps 1 to 5 are repeated for each sequence in B ($b_j \in B$), in order to create pair-wise consensus alignments of each sequence b_j and a_1:

Steps 1 and 2 are repeated for each pair-wise alignment extracted from the m MSAs of sequences a_1 and b_j and a directed graph containing the alignment information between a_1 and b_j is built:

Step 1 — For each alignment column i, that is not a gap in a_1', a node ($a_{1p}b_{jq}$) is created, if it does not already exist, containing the aligned amino acids of the alignment position $a_1'_i b_j'_i$, referring to sequence positions a_{1p} and b_{jq}. If $b_j'_i$ contains a gap, the created node depends on the first residue l in N-terminal direction.

Step 2 — For each pair of nodes $a_{1p}b_{jq}$ (refers to the alignment column $a_1'_i b_j'_i$) and $a_{1\ p+1}b_{j\ q+x}$ an edge with length one is created connecting both nodes. If this edge is already present in the graph, its weight is incremented by one.

Step 3 — Edge length is adapted for compatibility with Dijkstra's algorithm searching for the least-cost path: $m - (\text{edge weight} - 1)$.

Step 4 — Start and end nodes are introduced in the graph. The start node is connected with an edge of weight m to all nodes $a_{11}b_{jx}$, representing the first position of a_1. The end node is connected with en edge of weight m to all nodes $a_{1z}b_{jx}$, representing the last position of a_1.

Step 5 — With Dijkstra's algorithm we search for the least-cost path from start to end node, in order to construct the consensus alignment for sequences a_1 and b_j.

Step 6 — All consensus alignments are combined and anchored on sequence a_1. All residues of sequences in B not aligned to a_1 in the consensus alignments are added as insertions at the respective positions as lower case letters. Thus, the lower case letters do not represent aligned residues.

Position-wise plot of edge weights — The quality of the alignment between sequences A and B is determined by the least-cost path (see step 5). For each node on this path the maximum of the in- and outgoing edges is determined. The values for each column of the consensus alignment are averaged over all alignments separately for VDAC, Tom40, and Mdm10 sequences.

A graphical representation of our method applied to a few example sequences is shown in Supplementary Fig. S1. A flow chart of the pipeline for testing our consensus alignment procedure is shown in Supplementary Fig. S2.

2.7. Phylogeny

To reduce the complexity of tree reconstruction and to allow a more thorough search of the tree space, we extracted selected sequences of the multiple sequence alignment from organisms across the whole eukaryotic tree of life and removed sites were more than 5% of the sequences contained a gap, resulting in an alignment with 242 columns.

From this reduced alignment a maximum-likelihood phylogeny was reconstructed with RAxML v7.2.6 [68] using gamma-distributed rate heterogeneity and the LG substitution matrix, which is according to ProtTest [69] the best-fitting substitution matrix. Branch support values were calculated with RAxML's rapid bootstrap algorithm [70] from 1000 bootstrap trees using CAT approximation [71]. Additionally, a Bayesian tree search was performed with LG and CAT substitution matrices in PhyloBayes [72]. For the posterior probability estimation we ran four independent chains with a total length of 80,000 (LG) or 220,000 (CAT) cycles and checked the convergence by comparing their bipartitions (maxdiff < 0.1). The first 20,000 cycles were removed as burn-in and every second tree was used for the estimations. Finally, we compared both models using a 10-fold cross-validation test (10 replicates, 3000 cycles with a burn-in of 500 cycles) as implemented in PhyloBayes, based on the topology estimated by the CAT and LG model. The LG model has a better statistical fit (Table 2) no matter which topology was provided. The posterior probabilities obtained with the LG model were mapped onto our ML tree.

2.8. Clustering, homology modeling and molecular graphics

Sequence clustering was performed with CLANS [67] in 2D at a p-value cutoff of 0.1. To construct the score matrix, CLANS invoked BLAST [73] using the BLOSUM62 substitution matrix [74].

Homology models were built with MODELLER 9v7 [75]. The models were refined with YASARA (http://www.yasara.org) and its YAMBER3

Table 1
Explanation of defined symbols and indices for the construction of the consensus alignment.

Symbol	Description	Index	Description
a, b	Sequences	j	Sequence number
		p, q	Sequence positions
		z	Length of a sequence
a', b'	aligned sequences	i	Alignment column index
m	Number of MSAs		
n	Number of sequences		

Table 2
Cross-validation comparing the CAT and LG model.

Reference tree	Data set	Best model	Likelihood
LG	Complete	LG	65.796 ± 18.8941
LG	Rem[a]	LG	71.109 ± 26.4841
CAT	Complete	LG	63.862 ± 16.7783
CAT	Rem[a]	LG	79.586 ± 25.0824

[a] Without potential Mdm10 sequences of Glaucophyta and Heterolobosea.

force field [76]. Molecular graphics were created with Yasara (http://www.yasara.org) and PovRay (http://www.povray.org).

3. Results and discussion

3.1. Mdm10 has a VDAC-like fold

Searching the non-redundant (nr) protein database from NCBI with the 'eukaryotic porin' (PF01459) profile hidden Markov model (pHMM) that was built for the detection of Tom40 and VDAC sequences yields some Mdm10 protein sequences as significant hits (E-value < 0.01). Remarkably, other sequences not belonging to Tom40, VDAC or Mdm10 family were not detected within the search limits. Using the Mdm10 pHMM (PF12519) we detected also a Tom40 sequence of *Arabidopsis lyrata* as significant hit besides Mdm10 sequences. Consistent with the similarity of Mdm10 to eukaryotic porins, the VDAC-like fold [22–24] is the best match among all existing structural folds as determined by the servers HHPred [77], FFAS03 [78] and Phyre2 [79] (Supplementary Table S2). The second best hit is different for the three prediction server, has low confidence scores and a very low number of aligned residues in comparison to the VDAC hit (Supplementary Table S2). Both results suggest that Mdm10 belongs to the eukaryotic porin superfamily.

Next, we set out to embed Mdm10 into the structural context of eukaryotic porins by constructing a reliable multiple sequence alignment (MSA). We created a database composed of 'eukaryotic porins' including 76 fungal Mdm10 sequences. However, aligning VDAC and Tom40 sequences with standard MSA algorithms as, e.g., implemented in MAFFT [66] is challenging due to the high sequence divergence making the result highly dependent on the used parameters [9,80]. Addition of Mdm10 sequences to the dataset further increases the amount of possible alignments. Furthermore, construction of an alignment with, e.g., pHMM-based methods has the disadvantage that the underlying HMM is built from an MSA as well.

To overcome this problem we developed a graph-based algorithm that principally makes a majority decision and allows the alignment of divergent sequences to build a MSA of VDAC, Tom40 and Mdm10. The algorithm searches in a set of 1050 alignments, constructed with different input parameters by MAFFT [66], for the most frequent alignment (Fig. 1A). Our previous implementations focused on an alignment of the core region of regular secondary structure elements not including terminal regions of regular secondary structure and loops [9,80]. The most frequently occurring alignment of such a core region was extracted from a set of different MSAs. Our new method (Fig. 1A) builds graphs for all sequence pairs (Supplementary Fig. S1), where one member is mouse VDAC (*mm*VDAC, PDB: 3EMN), with the alignment information extracted from all 1050 MSAs each calculated with different parameter combinations. Aligned residues of both sequences correspond to the nodes, which – if they occur in the same MSA – are connected by an edge, weighted inversely proportional to its observed frequency ($1050 - \mathrm{freq}_{obs}$). With Dijkstra's algorithm for finding the path with the lowest cost in a graph [81] the most frequent pair-wise alignment for all sequence pairs is computed. At the end an MSA anchored at *mm*VDAC is constructed. We have successfully tested our consensus sequence alignment procedure and observed that in most cases a clear improvement in comparison to a single MAFFT MSA is achieved. We evaluated the performance of our method by aligning various pairs of protein domains from the SCOP/ASTRAL database [82,83] (http://scop.berkeley.edu/) belonging to different PFAM families, which were selected to reflect the situation within the eukaryotic porin superfamily; i.e. we specifically searched for pairs of protein domains with known structures, which have the same fold but strongly divergent sequences (Supplementary Fig. S3, Table S4).

In the consensus MSA of VDAC, Tom40 and Mdm10 we can assign 19 β-strands and the N-terminal helix to Mdm10 (Fig. 1B, Supplementary Fig. S4). The average frequencies of these secondary structure elements are higher within the VDAC family than between VDAC and Tom40 or VDAC and Mdm10 (Fig. 1C). This can be explained as the consensus MSA is constructed with mmVDAC (PDB: 3EMN) as the reference, and alignments within a protein family are less difficult than between different families as the result of the sequence divergence. In general, we observe a higher frequency for regular secondary structure elements than for loop regions (Fig. 1C). The N-terminal part of the β-barrel is less conserved between Tom40, VDAC, and Mdm10 than the C-terminal region (Fig. 1C). Such a difference in the degree of conservation was also observed for Omp85-like β-barrels [32]. Summarizing our results we can conclude that Mdm10 is a β-barrel protein and belongs to the superfamily of eukaryotic porins.

3.2. Mdm10 exposes large loops to the cytosol and intermembrane space of mitochondria

Based on our consensus MSA and the result of structure prediction we built a homology model of Mdm10 from *S. cerevisiae* (scMdm10) with mmVDAC (PDB: 3EMN) as template (Fig. 2A). The model shows the typical properties of a transmembrane β-barrel with β-strands of mostly alternating hydrophobicity meaning that hydrophobic residues point to the lipid phase and hydrophilic residues are present in water-accessible positions (Supplementary Fig. S5). Interestingly, based on the model, scMdm10 exposes long loops on both sides of the membrane (Fig. 2A). Such loops are absent in Tom40 and in porin, the VDAC homolog in yeast (Fig. 2A), which indicates a functional specialization of Mdm10. In scMdm10 a single elongated loop (L18) is on one side and three are on the other side of the β-barrel (L3, L9, L15) with L9 being a rather short loop. Similar loops exist for example in FadL (PDB: 1T1L), which contains loops up to ~30 amino acids long [84], or TonB-dependent transporters, which exhibit loops of up to ~50 amino acids in length connecting the transmembrane β-strands (e.g. PDB: 3CSL; [85]).

Analyzing the loops in other fungal Mdm10 sequences, we noticed that the frequency of long loops increases from basal Fungi up to Dikarya (Fig. 2B). In general, these long loops are of disordered nature as predicted by the GeneSilico metaserver [86]. Loop L3 is an exception as it has only low disorder content, especially in Dikarya (Fig. 2B). In silico analyzes suggest that in the absence of a selection pressure long disordered regions are quickly lost during evolution [87] and existing disordered regions are discussed as protein interaction hubs [88–91]. Thus, we addressed the topology and the role of the loop region of the yeast *S. cerevisiae* Mdm10 experimentally.

3.3. The topology of the Mdm10 loops in mitochondria

We generated yeast strains expressing Mdm10 variants, in which the loops were deleted individually (Fig. 3A). All Mdm10 loop deletion mutants grew normally on non-fermentable medium compared to wild-type (Supplementary Fig. S6A). Since Mdm10 deletion mutants cannot grow on non-fermentable medium [40,92] we conclude that the individual loops of Mdm10 are not essential for the function of the protein. Similar levels of Mdm10 were detected in mutant and wild-type mitochondria (Supplementary Fig. S6B). The signal for Mdm10ΔL3 (hereafter ΔL3) appeared to be reduced due to detection problems with our Mdm10-specific antibody (Supplementary Fig. S6B).

For topology studies wild-type, Mdm10ΔL15 (hereafter ΔL15) and Mdm10ΔL18 (hereafter ΔL18) mitochondria were either left intact or the outer membrane was ruptured by osmotic swelling and subsequently treated with proteinase K. Mdm10 proteins and their fragments were detected on a SDS-PAGE by immunodecoration with Mdm10-specific antibodies (Fig. 3B). The specificity of the immuno-detected signals was confirmed by comparison with mitochondria devoid of Mdm10 (Supplementary Fig. S6C). In intact

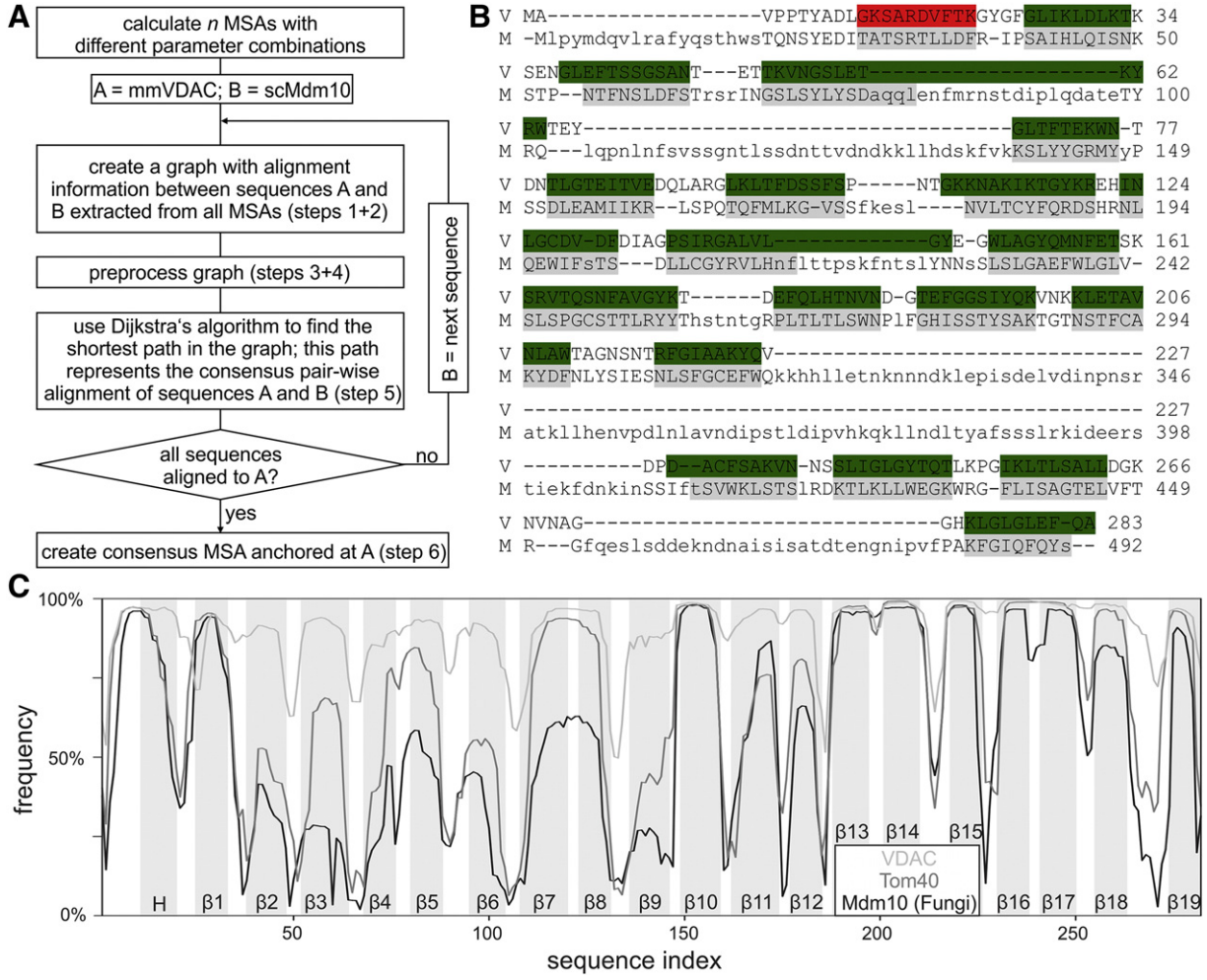

Fig. 1. Consensus alignment. (A) A schematic representation of our alignment procedure is shown. For all possible pairs of mmVDAC (sequence a_1) with all other sequences (sequence b_j) the alignment information is extracted from all m calculated MSAs ($m = 1050$) and a graph is constructed with this information (steps $1 + 2$). After this, the graph is prepared for applying the Dijkstra algorithm (step $3 + 4$) [81] and by this algorithm the highest scoring pair-wise alignment of sequences a_1 and b_j is determined (step 5). As a last step all pair-wise alignments are combined (step 6). For a detailed explanation of the single steps, please, see Material and methods and Supplementary Fig. S1. (B) Consensus alignment of mmVDAC (V; PDB: 3EMN) and scMdm10 (M). Red marks the α-helix and green the β-strands of mmVDAC and gray the secondary structure elements of scMdm10 derived by our alignment procedure. Numbers on the right indicate the position of the last amino acid in the corresponding sequence. (C) In total 1050 different multiple sequence alignments of a combined set of VDAC (light gray), Tom40 (dark gray), and Mdm10 (black) amino acid sequences were calculated with MAFFT as described in Material and methods. By a graph algorithm for finding the least-cost path [81] a consensus alignment was constructed. The average frequency of the chosen edge between two neighboring, aligned residue pairs along the least-cost path is shown. Plotted is the sequence position in the template against the average frequencies of the alignment between template mmVDAC (PDB: 3EMN) and all target sequences of the respective protein family. In short, a low frequency (low support) implies that the respective sequence positions are quite dissimilar and thus difficult to align to the template VDAC. In contrast, a high frequency (strong support) indicates a well-supported alignment due to the higher degree of similarity of the aligned positions.

wild-type mitochondria only a fragment of less than 5 kDa is removed from Mdm10 by the protease (Fig. 3B, lane 2, F1). After hypoosmotic swelling Mdm10 became accessible to proteinase K and a digestion product of 10 kDa size was detected (Fig. 3B, lane 4, F2). Thus, only a small portion of Mdm10 is exposed to the cytosol, whereas the protein is largely accessible from the intermembrane space side.

The analyses of the mutant strains indicated that ΔL18 was protected from externally added proteases in intact mitochondria and was only degraded upon osmotic swelling. In contrast, ΔL15 was already accessible to proteinase K in intact mitochondria (Fig. 3B, lanes 5–12). The control protein Tom70 was already degraded in intact mitochondria, whereas the intermembrane space-exposed Tim23 and Tim10 became accessible to the protease only upon osmotic swelling (Fig. 3B, lower panels). We conclude that loop 18 of Mdm10 is exposed to the cytosol, whereas the other three loops face the intermembrane space side (Supplementary Fig. S6D). Supporting this view, a C-terminal portion of Mdm10 was degraded in intact mitochondria by proteinase K as shown by degradation of a His-tag fused C-terminally to full length Mdm10 (Fig. 3C, lane 2).

For comparison porin (VDAC) does not expose protease-accessible loops to either side of the membrane [22–24] and was resistant to proteinase K treatment (Fig. 3D, second panel). Also Tom40 was protected against proteolytic cleavage in intact mitochondria, but was partially digested after rupturing the outer membrane (Fig. 3D, first panel). The resistance of VDAC and Tom40 to protease treatment before mitochondrial swelling is consistent with the absence of long, cytosolic loops [9,22–24]. The slight reduction of the molecular weight of Tom40 by protease treatment after swelling most likely reflects the removal of the unstructured N-terminal region [9].

3.4. The role of the Mdm10 loops in mitochondrial biogenesis

We asked whether interactions of Mdm10 with ERMES, SAM or Tom7 were affected by deletion of the loop regions. Steady state levels of other ERMES or SAM subunits and of other outer membrane proteins were similar to wild-type mitochondria (Supplementary Fig. S6B). To study the formation of the ERMES complex we introduced the Mdm10 variants in yeast strain expressing Protein A-tagged Mmm1 and used

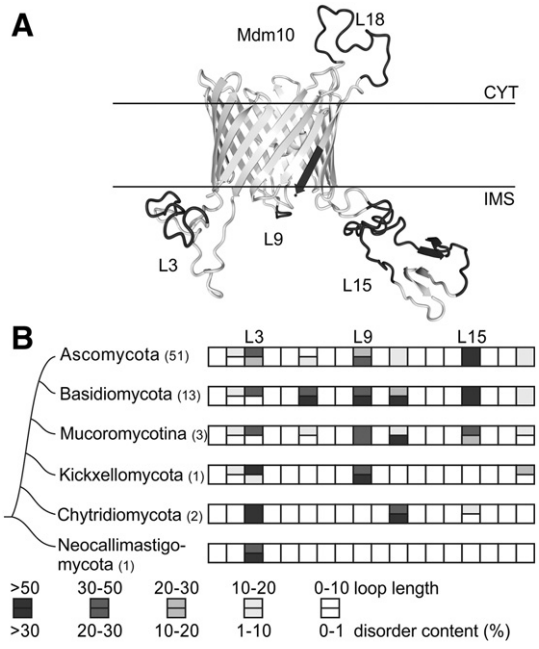

Fig. 2. The homology model and topology of Mdm10 from yeast. (A) Homology models of VDAC, Tom40 and Mdm10 from *Saccharomyces cerevisiae* are shown embedded in a schematic membrane. The models are colored in light gray. Sequence regions before the N-terminal helical region (Tom40, Mdm10) were not modeled, because they are not present in the template structure mmVDAC (PDB: 3EMN). Residues predicted as disordered by the GeneSilico metaserver (consensus prediction; https://genesilico.pl/meta2; [86]) are colored in dark gray. (B) The loops connecting the transmembrane β-strands are depicted as squares and labeled from left to right (that is from N- to C-terminus) as L1 to L18. The upper half of a box encodes the average length and the lower half the average predicted disorder content of the respective loop calculated with IUpred [108]. If the colors encoding the length and disorder content of a loop are the same, a box is not split. The average length and disorder content of each loop are shown in different shades of gray (indicated in the figure) for each phylum of Fungi, in which Mdm10 was detected. The relations of these Mdm10-containing groups are indicated in a schematic tree. The number of sequences for each phylum is given in brackets.

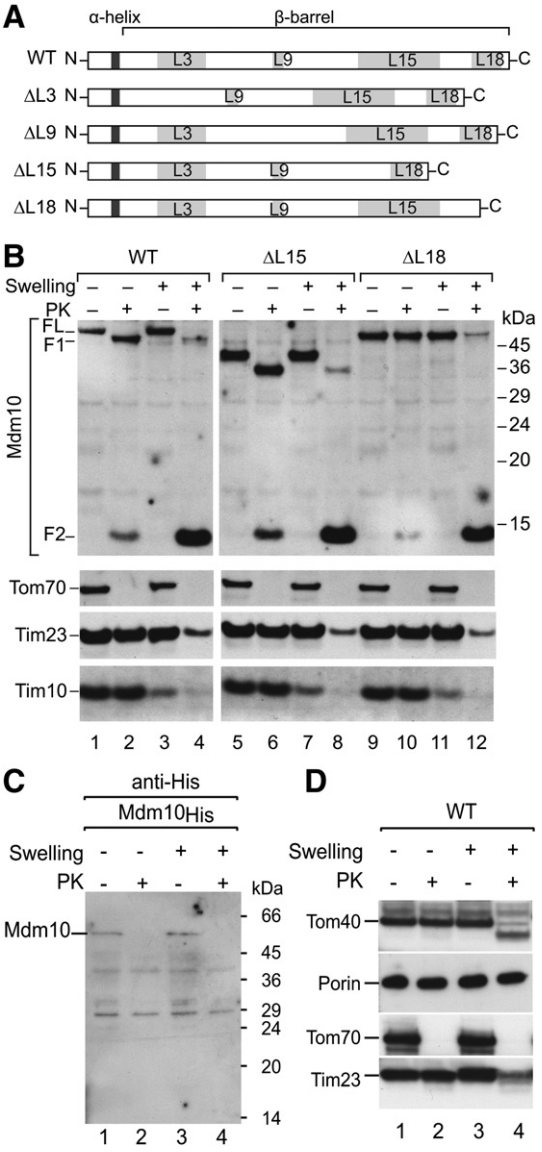

Fig. 3. Topology of yeast Mdm10. (A) Scheme of the Mdm10 loop deletion mutants. Light gray bars indicate the loop segments, medium gray bars the α-helix, and the black bar the C-terminal His-tag. (B) Mitochondria from wild-type (WT) or the indicated Mdm10 loop deletion mutant were ruptured by osmotic swelling or left intact and subsequently incubated in the presence or absence of proteinase K. Mitochondrial proteins were separated by SDS-PAGE followed by Western Blotting and immunodetection with the indicated antibodies. FL full length Mdm10; F1, F2 — proteolytic fragments of Mdm10. (C) and (D) $Mdm10_{His}$ and wild-type mitochondria were treated as described under (B). Mitochondrial proteins were separated by SDS-PAGE and detected by Western Blot and immunodecoration with the indicated antisera.

total cell extract for affinity purification via the Protein A-tag. ΔL3, ΔL15 and ΔL18 were co-purified with Mmm1 (Fig. 4A). Mdm12 and Mdm34 were eluted with the same efficiency like in wild-type strain indicating that the ERMES was formed in all Mdm10 loop deletion mutants (Fig. 4A). Other mitochondria proteins were not co-purified with Mmm1-ProtA (Fig. 4A).

To probe for an association of Mdm10 with either the SAM complex or Tom7 we lysed mitochondria isolated from individual loop deletion mutants with digitonin and analyzed Mdm10-containing complexes by BN-PAGE (Fig. 4B). We detected the SAM-Mdm10 complex at 350 kDa and the Mdm10-Tom7 pool at about 140 Da [38,44,45,93] in all strains analyzed (Fig. 4B, lanes 6–8). The weaker signal in ΔL3 was most likely due to the reduced recognition efficiency by the Mdm10 antibody, which was supported by the wild-type-like level of Mdm10-SAM complex detected with antibodies against Sam50 (Fig. 4C, lanes 1–4). Additionally, in Mdm10ΔL3 mitochondria some unassembled Mdm10 was detected indicating that the absence of loop 3 might partially disturb biogenesis of Mdm10 (Fig. 4B, lanes 1–6). Since Mdm10 plays an important role in the formation of the mature TOM complex we analyzed the biogenesis of the TOM complex in the mutant strains. The amount of the TOM complex was comparable in the mutant and wild-type mitochondria (Fig. 4C, lanes 5–8). To study the Tom40 assembly we imported radiolabeled Tom40 into the mitochondria isolated from the Mdm10 mutant strains. Imported Tom40 is assembled into the TOM complex via two intermediate stages, which can be resolved by blue native electrophoresis [27,30]. Both intermediate stages as well as the mature TOM complex were efficiently formed in the Mdm10 mutant mitochondria (Fig. 4D). We conclude that the role of Mdm10 in the biogenesis of the TOM complex is not compromised by individual deletion of any loop.

3.5. The unique features of the β-barrel of Mdm10

We have shown that the individual loop regions of Mdm10 are not important for the known interactions and functions of the protein. Consequently, specific features of the β-barrel might be important for Mdm10. We analyzed sequence properties of fungal Mdm10 in the structural context of our homology model of scMdm10. Characteristic for a VDAC-like fold is a 19-stranded β-barrel and an N-terminally located helix [9,22]. In VDAC and Tom40 the latter is amphiphilic and is attached to a hydrophobic face of the pore interior [9,22]. At the base of the binding pocket in the pore of Tom40 and VDAC are two residues with conserved tiny

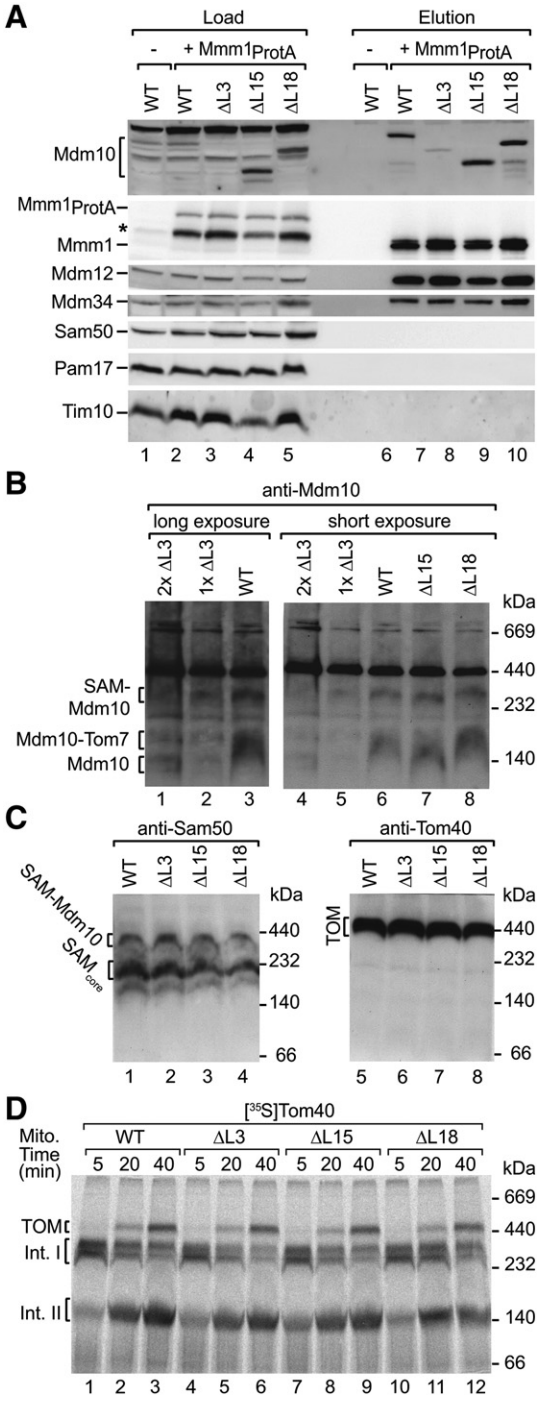

Fig. 4. Characterization of Mdm10 loop deletion mutants. (A) Total extract of Mdm10 loop deletions in the Mmm1Protein A background were lysed with digitonin and used for affinity purification via the Protein A-tag of Mmm1. Load (4.5%) and elution (100%) fractions were subjected to SDS-PAGE, Western Blotting and immunodetection with the indicated antisera. Asterisk marks unspecific band detected by Mmm1-specific antibodies. (B) Mitochondria from wild-type or the indicated Mdm10 loop deletion mutants were lysed with digitonin and analyzed by blue native electrophoresis and immunodetection with Mdm10-specific antiserum. (C) Wild-type and Mdm10 loop deletion mutant mitochondria were lysed with digitonin and subjected to blue native electrophoresis. Protein complexes were detected by immunodecoration with the indicated antisera. (D) Radiolabeled Tom40 was imported into wild-type and Mdm10 loop deletion mitochondria. Mitochondria were lysed with digitonin and ^{35}S-labeled Tom40 containing intermediates were separated by blue native electrophoresis and detected by autoradiography.

sidechains (scTom40: G270, G304; scPor1: A203, A222; [9]). Only one of these two residues is conserved in Mdm10 as well (Gly 100%; scMdm10: Gly310). The other position is generally occupied by amino acids with small side chains (Cys 51.28%, Ala 28.21%, Ser 20.51%; scMdm10: Cys293). Due to the presence of a residue with a larger side chain the mode of interaction of the N-terminal helix with the pore wall might differ from Tom40 and VDAC.

In addition, Tom40 contains a "polar slide" comprising polar residues lined by two hydrophobic patches within the N-terminal region (β3–β8), whereas in VDAC this part is composed of mainly hydrophilic residues [9]. The corresponding region in Mdm10 contains extensive hydrophobic patches and less hydrophilic residues than Tom40 and VDAC (Fig. 5A) forming a hydrophobic surface in the region of β-strands β3 to β8. Based on the model Mdm10 would be able to form a pore with diameter similar to the pore of VDAC or Tom40 (Fig. 2A). In this scenario the presence of hydrophobic patches would lead to different properties of the putative Mdm10 pore in comparison to the pores formed by Tom40 or VDAC. Consequently, in case Mdm10 is directly responsible for substrate transport, the latter likely differs from those of the other members of the eukaryotic porin superfamily.

The multitude of contacts of Mdm10 to ERMES, SAM or TOM components prompted us to analyze the membrane-exposed surface of the β-barrel for positions of conserved amino acid residues, which might indicate putative interaction surfaces [94]. We observed that an extended surface groove on β-strands β4 and β5 is formed by two residues with conserved tiny and small side chains, i.e. G144 (Gly 89.74%, Ala 7.69%, and Ser 2.56%) and A155 (Ala 76.92%, Gly 20.51%, and Ser 2.56%; Fig 5B). Two conserved aromatic residues with large side chains in β-strand β3 are directly adjacent. These properties are conserved throughout the whole Tom40 family as well (Fig. 5C) but not in the VDAC family. A second region of high conservation within the Mdm10 family only is located on the opposite side of the β-barrel and spans the membrane as a thin strip containing five conserved aromatic residues in β-strands β11 to β14 (Fig 5D).

The functions of these regions are unknown, however, they could act as protein binding regions. The strength of the conservation of the membrane-spanning strip of aromatic residues strongly hints at a protein–protein interaction surface [94]. The other putative binding site is alike in Tom40 and Mdm10, which might hint at a similar substrate. In this respect it is of interest to note that Tom7 was shown by site-directed cross-linking to interact via the same interface with Mdm10 and Tom40 [45], indicating a similar binding site on both β-barrel proteins; a putative candidate is the region of β3–β5 in Mdm10 and Tom40. Supporting this notion the same pattern of amino acids is not conserved in VDAC, which does not interact with Tom7.

3.6. Evolution of Mdm10

β-barrels evolved by duplication events from an ancestral β-hairpin and represent an extreme example of divergent evolution [95]. Thus, it appears unlikely that the 19-stranded β-barrel fold of the eukaryotic porin superfamily evolved more than once by convergent evolution. Especially the fact that all other structurally known transmembrane β-barrel folds have an even number of β-strands makes it unlikely that the same evolutionary pressure leading to the 19-stranded β-barrel fold occurred more than once.

So far, our analyses have shown that Mdm10 is similar to the eukaryotic porin superfamily in sequence and structure. To explore the phylogenetic relationship we reconstructed a maximum likelihood (ML) tree and performed a Bayesian tree search based on our consensus MSA of VDAC, Tom40 and Mdm10 of selected organisms (Fig. 6). We have calculated an unrooted tree, because the direct predecessor of the eukaryotic porin superfamily has not yet been identified.

In general, there is a well-supported split between the Tom40/Mdm10 and VDAC sequences (bootstrap/posterior probability of 100/1.0). Furthermore, all Mdm10 sequences lie on the same branch (bootstrap/posterior probability of 87/0.99), whereas the Tom40 branch of the ML tree is not supported leading to several Tom40

branches. The succession of the kingdoms of Fungi, Metazoa and Viridiplantae is correct [96] in the VDAC and Tom40 branches (Fig. 6). The Mdm10 clade originates at the base of Tom40; however, this positioning is not well supported. Surprisingly, sequences from Amoebozoa and *Capsaspora owczarzaki* (Filasterea) are grouped together with the Mdm10 sequences of Fungi, which is supported by good values for bootstrap (87) and posterior probability (0.99). Thus, most probably the occurrence of Mdm10 is not limited to Fungi. In contrast, Mdm10 cannot be identified in Metazoa or plants.

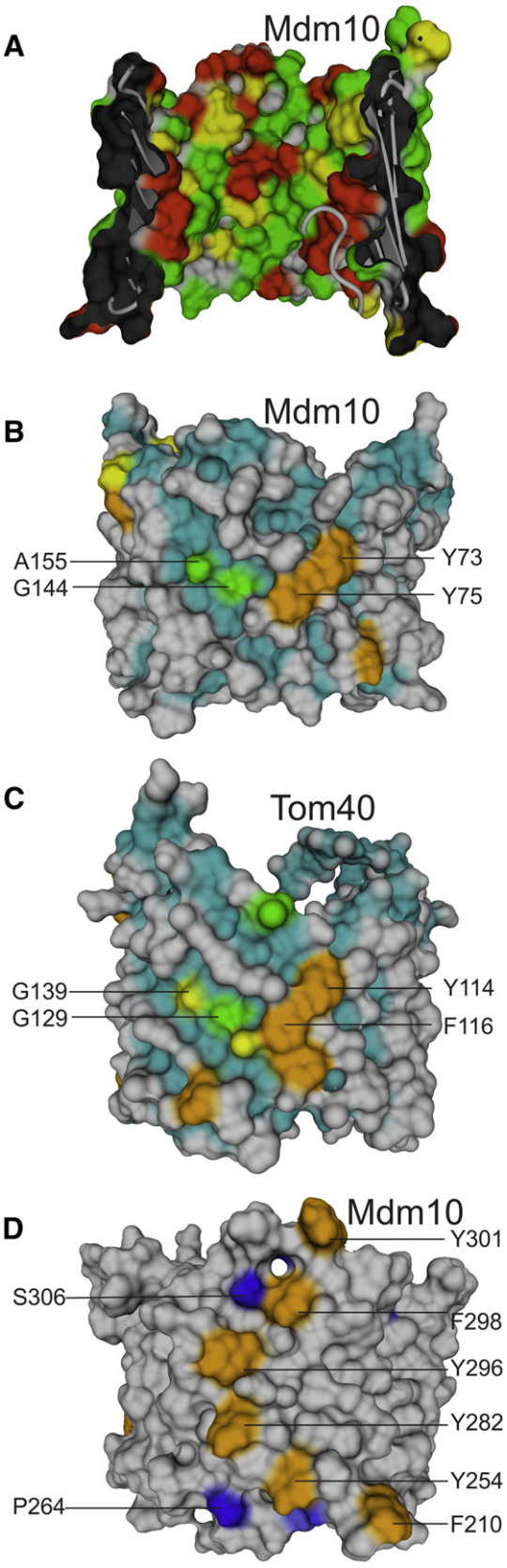

Fig. 5. Conserved features of Mdm10. (A) The homology model of scMdm10 was cut open to show the pore interior. Sidechain atoms are colored by the average hydrophobicity [109] derived from all amino acids in the corresponding columns of the in here constructed consensus MSA, backbone atoms are colored gray. On average strongly hydrophilic positions (−4.5 to −1.6) are colored in red, average medium hydrophilicity (−1.6 to −0.4) in yellow, and on average hydrophobic positions (−0.4 to 4.5) are colored green. See left panel of figure 4a, b in [9] for comparison to the corresponding region in Tom40 and VDAC, respectively. (B-D) Side views of the homology model of (B, D) scMdm10 and (C) scTom40 are shown as surface representation. Properties derived for Mdm10 or Tom40 sequences (max. sequence identity 70%, in case of Mdm10 after removal of long loops to avoid artifacts) from the consensus alignment were mapped onto the surface. The long loops of scMdm10 were hidden for the sake of clarity. (B, C) Conserved aromatic residues are colored in orange, backbone atoms are colored in cyan, sidechain atoms of residues with conserved tiny or small sidechains are colored in green and yellow, respectively. (D) Residues conserved in 70% of Mdm10 sequences are shown in color. Conserved aromatic residues are colored in orange, others in blue.

3.7. The ERMES complex and Mdm10 emerged early in eukaryotic evolution

In order to support the phylogenetic classification of the potential Amoebozoa and Filasterea sequences as Mdm10, we took a different approach and analyzed the evolutionary occurrence of those proteins, which form complexes with Mdm10. Mdm10 was reported to interact with the SAM and ERMES complex. Therefore, we tested whether Mdm10 occurs concomitantly with its interaction partners. Sam50 is generally found in all eukaryotes [33], whereas Mdm10 does not exist in Metazoa and plants. Further, the SAM components Sam35 and Sam37 were identified in Fungi, Metazoa and plants as well [58,97–101]. Thus, the general components of the SAM complex are present in most eukaryotes and their occurrence is not linked to the presence of Mdm10.

The ERMES component Gem1 is present in nearly all eukaryotes (Table 3, Supplementary Fig. S7). Thus, Gem1 might not exclusively be linked to an Mdm10-containing mitochondria-ER tether. Moreover, the formation of stable ERMES complexes does also take place in the absence of Gem1 [46,57]. Thus, Gem1 might exert a rather regulatory function in the ERMES complex than being a structural core component [46,102].

For the ERMES complex we also studied the occurrence of Mmm1, Mdm12 and Mdm34 (Fig. 7, Table 3). Like Mdm10, all three are non-existent in Metazoa and plants, whereas they are detectable in all Mdm10-containing systematic groups. Thus, we found that the complete ERMES complex is not only present in Fungi but also in Amoebozoa and Filasterea, and we conclude that the potential Mdm10 sequences in Amoebozoa and Filasterea indeed belong to the Mdm10 family.

While almost nothing is known about the mitochondria-ER tethers in plants [103], it is discussed that proteins like mitofusin-2 (Mfn2; [104]), Bap31/Fis1 [105] or IP3R/Grp75/VDAC [106] might contribute to ER-mitochondria linkage in mammals. Interestingly, Filasterea contain both ERMES and Mfn2, whereas prior to Filasterea Mfn2 is not present (Fig. 7, Table 3). Thus, different mitochondrial-ER tethers have evolved in the different branches of life, and it could be that in Metazoa Mfn2 replaced ERMES with respect to its ER-mitochondria linkage function. Metazoa and plants also contain proteins, which were recognized by the TULIP pHMMs of Mmm1, Mdm12 and Mdm34 (Fig. 7B; unlabeled dots), but their sequence similarity is below the used threshold of 1E−15 and the function of these proteins is not annotated. Furthermore, the average length of the proteins differs (ERMES: 489.36; other TULIP/SMP: 936.60) and the other TULIP/SMP proteins often contain additional PFAM domains like C2 (PF00168), C1_1 (PF00130), PDZ_2 (PF13180) or

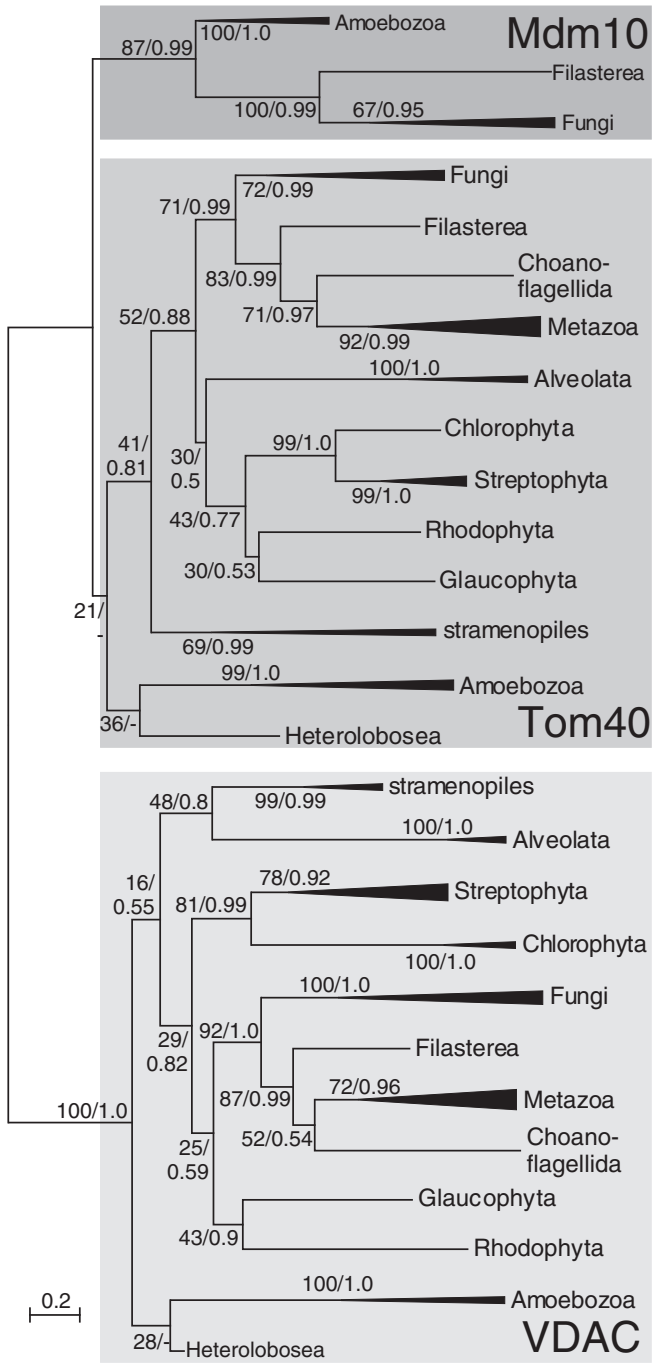

Fig. 6. Phylogeny of the eukaryotic porin superfamily. A maximum likelihood (ML) phylogeny of the eukaryotic porin superfamily, containing VDAC, Tom40 and Mdm10 was calculated with RAxML and the LG substitution model. Bootstrap values and posterior probabilities were mapped onto the ML tree. A "-" refers to splits, which are not supported by the Bayesian consensus tree with a cutoff of 50%. Subtrees were collapsed with MEGA5 [110] for a simplified representation.

PH (PF00169) and, interestingly, also Fungi contain these additional TULIP/SMP proteins with unknown function (Fig. 7B; square dots which are not highlighted). All in all, the detected TULIP/SMP sequences in Metazoa and plants most likely have a function distinct from the ERMES components.

Interestingly, *Naegleria gruberi* (Heterolobosea) contains the three ERMES components Mmm1, Mdm12, and Mdm34 as well. For *N. gruberi* our data set comprises a third eukaryotic porin-like sequence, which is according to Bayesian analysis with a posterior probability of 0.86 (LG)/0.94 (CAT) a member of the Mdm10 family (Supplementary Fig. S8). Together with the presence of other ERMES components this sequence is most likely the Mdm10 in *N. gruberi*. In the recent release of the genome of *Cyanophora paradoxa*, a glaucophyte at the base of the Archaeplastida [107], we also discovered ERMES components with a TULIP domain and a third eukaryotic porin-like sequence. The location of this sequence in the Mdm10 subtree is weakly supported by the ML analysis, but in the Bayesian analysis with the CAT model it is supported with a probability of 0.94, and in conjunction with the presence of other ERMES components (Table 3) this sequence is the best candidate for Mdm10 in *C. paradoxa*. Thus, ERMES and Mdm10 appear concomitantly during eukaryotic evolution. We also detected putative Mdm12 and Mdm34 sequences in Euglenozoa and Parabasalia. However, it remains to be investigated whether an ancient, highly divergent Mdm10 and also an Mmm1 homolog are present in mentioned systematic groups.

Table 3
Evolution of the ERMES complex.

Species	Gem1	Mdm10	Mdm34	Mdm12	Mmm1	Mfn2	Sam50
Euglenozoa	−	−	+	+	−	−	+
Heterolobosea	+	+	+	+	+	−	+
Parabasalia	−	−	+	+	−	−	+
Mycetozoa (Amoebozoa)	+	+	+	+	+	−	+
Filasterea	+	+	+	+	+	+	+
Fungi	+	+	+	+	+	−	+
Metazoa	+	−	−	−	−	+	+
Glaucophyta	−	+	−	+	+	−	+
Viridiplantae	+	−	−	−	−	−	+

By HMM searches with hmmer (http://hmmer.janelia.org) we scanned the non-redundant (nr) database (NCBI) and genomes of species not integrated in the nr database for the presence of components of the ERMES and SAM complex. The presence of such a component is indicated by '+', a '−' means 'not detected'. GenBank IDs of sequences identified in early branching eukaryotes are given in Supplementary Table S3.

4. Conclusions

We have identified Mdm10 as a member of the eukaryotic porin superfamily, which also includes Tom40 and VDAC. We developed a new consensus MSA approach, which results in a reliable alignment of different protein families with the same fold. Subsequently, we show by homology modeling and proteolysis experiments that scMdm10 unlike VDAC and Tom40 exposes large loops to both sides of the membrane. However, characterization of single-loop deletion mutants of scMdm10 revealed that the loops are not required for Mdm10 function. An analysis of the MSA in the structural context of the homology model of scMdm10 revealed conserved spots on the membrane-exposed surface of the β-barrel, one of which is also present in the Tom40 family. In future research these sites can now be probed specifically for their involvement in protein–protein interactions, e.g., with Tom7. Mdm10 and other ERMES core components like Mdm12, Mdm34 and Mmm1 are not only present in Fungi, but, surprisingly, are also present in some protist groups like Filasterea, Amoebozoa and Heterolobosea, and are lost in Metazoa and Viridiplantae. In contrast, the SAM complex is present in all eukaryotes. Thus, we conclude that Mdm10 and other ERMES core components occur concomitantly in unikonts as well as bikonts and that the function of Mdm10 in the ERMES complex evolved at an early stage of evolution. All together, our data support the view that Mdm10 is a central part of the ERMES complex.

Acknowledgements

We are grateful to Ingo Ebersberger for stimulating discussions regarding phylogenetic analyses and helpful comments on the manuscript. We thank Prof. Dr. Nikolaus Pfanner, Dr. Nils Wiedemann and Dr. Bernard Guiard for discussion and material. We thank Nicole Zufall for expert technical assistance. NF was funded by a fellowship

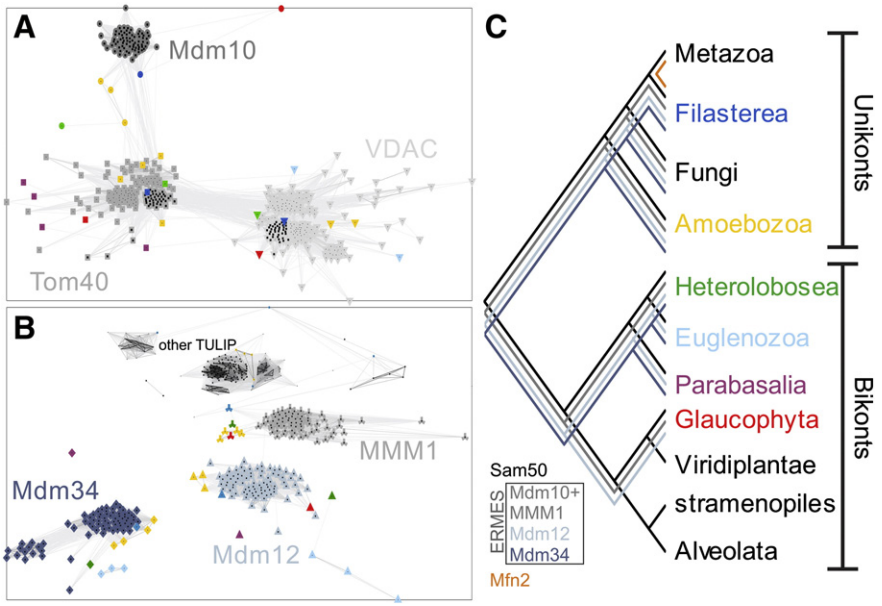

Fig. 7. Concerted evolution of Mdm10 and ERMES. A Clustering of (A) VDAC, Tom40, and Mdm10 or (B) Mdm12, Mdm34, Mmm1, and other closely related members with a TULIP domain (labeled with "other TULIP") was performed with CLANS. Sequences (dots) belonging to the same family share the same symbol. Early branching eukaryotes are highlighted by color as assigned in c. Connections between dots indicate the degree of sequence similarity by different shades of gray; the darker the more similar the linked sequences are. The p-value cutoff for displaying the similarity is (A) <1E−7 or (B) <1E−15. (C) A schematic representation of the eukaryotic tree, which was adapted from [111,112] is shown. The presence of ERMES (Mdm10 + Mmm1 in gray, Mdm12 in light blue, Mdm34 in dark blue), Mfn2 (orange), and SAM (Sam50 in black) throughout the eukaryotic tree is indicated by differently colored lines.

from CMP and TRAM. The project was funded by Volkswagenstiftung and Deutsche Forschungsgemeinschaft in the frame of CEF and SFB807 project 17 to ES. The work by TB was funded by the Deutsche Forschungsgemeinschaft, Sonderforschungsbereich 746 and the Excellence Initiative of the German Federal & State Governments (EXC 294 BIOSS).

Appendix A. Supplementary data

Supplementary data to this article can be found online at http://dx.doi.org/10.1016/j.bbamcr.2013.10.006.

References

[1] T.A. Richards, J.M. Archibald, Cell evolution: gene transfer agents and the origin of mitochondria, Curr. Biol. 21 (2011) R112–R114.
[2] F. Alcock, A. Clements, C. Webb, T. Lithgow, Evolution. Tinkering inside the organelle, Science 327 (2010) 649–650.
[3] E. Schleiff, T. Becker, Common ground for protein translocation: access control for mitochondria and chloroplasts, Nat. Rev. Mol. Cell Biol. 12 (2011) 48–59.
[4] M.T. Ryan, N.J. Hoogenraad, Mitochondrial-nuclear communications, Annu. Rev. Biochem. 76 (2007) 701–722.
[5] J.-C. Martinou, R.J. Youle, Mitochondria in apoptosis: Bcl-2 family members and mitochondrial dynamics, Dev. Cell 21 (2011) 92–101.
[6] A. Schneider, Mitochondrial tRNA import and its consequences for mitochondrial translation, Annu. Rev. Biochem. 80 (2011) 1033–1053.
[7] A. Toulmay, W.A. Prinz, Lipid transfer and signaling at organelle contact sites: the tip of the iceberg, Curr. Opin. Cell Biol. 23 (2011) 458–463.
[8] D.C. Bay, M. Hafez, M.J. Young, D.A. Court, Phylogenetic and coevolutionary analysis of the β-barrel protein family comprised of mitochondrial porin (VDAC) and Tom40, Biochim, Biophys. Acta 1818 (6) (2012) 1502–1519.
[9] D. Gessmann, N. Flinner, J. Pfannstiel, A. Schlosinger, E. Schleiff, S. Nussberger, O. Mirus, Structural elements of the mitochondrial preprotein-conducting channel Tom40 dissolved by bioinformatics and mass spectrometry, Biochim. Biophys. Acta 1807 (2011) 1647–1657.
[10] M. Pusnik, F. Charriere, P. Maser, R.F. Waller, M.J. Dagley, T. Lithgow, A. Schneider, The single mitochondrial porin of *Trypanosoma brucei* is the main metabolite transporter in the outer mitochondrial membrane, Mol. Biol. Evol. 26 (2009) 671–680.
[11] K. Zeth, Structure and evolution of mitochondrial outer membrane proteins of beta-barrel topology, Biochim. Biophys. Acta 1797 (2010) 1292–1299.
[12] M. Wojtkowska, M. Jakalski, J.R. Pienkowska, O. Stobienia, A. Karachitos, T.M. Przytycka, J. Weiner, H. Kmita, W. Makalowski, Phylogenetic analysis of mitochondrial outer membrane ss-barrel channels, Genome Biol. Evol. 4 (2012) 110–125.
[13] C.M. Koehler, New developments in mitochondrial assembly, Annu. Rev. Cell Dev. Biol. 20 (2004) 309–335.
[14] P. Dolezal, V. Likic, J. Tachezy, T. Lithgow, Evolution of the molecular machines for protein import into mitochondria, Science 313 (2006) 314–318.
[15] W. Neupert, J.M. Herrmann, Translocation of proteins into mitochondria, Annu. Rev. Biochem. 76 (2007) 723–749.
[16] T. Endo, K. Yamano, Multiple pathways for mitochondrial protein traffic, Biol. Chem. 390 (2009) 723–730.
[17] R. Benz, Permeation of hydrophilic solutes through mitochondrial outer membranes: review on mitochondrial porins, Biochim. Biophys. Acta 1197 (1994) 167–196.
[18] T. Hodge, M. Colombini, Regulation of metabolite flux through voltage-gating of VDAC channels, J. Membr. Biol. 157 (1997) 271–279.
[19] T. Salinas, A.-M. Duchene, L. Marechal-Drouard, Recent advances in tRNA mitochondrial import, Trends Biochem. Sci. 33 (2008) 320–329.
[20] E.H.Y. Cheng, T.V. Sheiko, J.K. Fisher, W.J. Craigen, S.J. Korsmeyer, VDAC2 inhibits BAK activation and mitochondrial apoptosis, Science 301 (2003) 513–517.
[21] K.S. McCommis, C.P. Baines, The role of VDAC in cell death: friend or foe? Biochim. Biophys. Acta 1818 (2012) 1444–1450.
[22] R. Ujwal, D. Cascio, J.-P. Colletier, S. Faham, J. Zhang, L. Toro, P. Ping, J. Abramson, The crystal structure of mouse VDAC1 at 2.3 A resolution reveals mechanistic insights into metabolite gating, Proc. Natl. Acad. Sci. U. S. A. 105 (2008) 17742–17747.
[23] M. Bayrhuber, T. Meins, M. Habeck, S. Becker, K. Giller, S. Villinger, C. Vonrhein, C. Griesinger, M. Zweckstetter, K. Zeth, Structure of the human voltage-dependent anion channel, Proc. Natl. Acad. Sci. U. S. A. 105 (2008) 15370–15375.
[24] S. Hiller, R.G. Garces, T.J. Malia, V.Y. Orekhov, M. Colombini, G. Wagner, Solution structure of the integral human membrane protein VDAC-1 in detergent micelles, Science 321 (2008) 1206–1210.
[25] G.E. Schulz, The structure of bacterial outer membrane proteins, Biochim. Biophys. Acta 1565 (2002) 308–317.
[26] A. Harsman, V. Kruger, P. Bartsch, A. Honigmann, O. Schmidt, S. Rao, C. Meisinger, R. Wagner, Protein conducting nanopores, J. Phys. Condens. Matter 22 (2010) 454102.
[27] J. Qiu, L.-S. Wenz, R.M. Zerbes, S. Oeljeklaus, M. Bohnert, D.A. Stroud, C. Wirth, L. Ellenrieder, N. Thornton, S. Kutik, S. Wiese, A. Schulze-Specking, N. Zufall, A. Chacinska, B. Guiard, C. Hunte, B. Warscheid, M. van der Laan, N. Pfanner, N. Wiedemann, T. Becker, Coupling of mitochondrial import and export translocases by receptor-mediated supercomplex formation, Cell 154 (2013) 596–608.
[28] V. Kozjak, N. Wiedemann, D. Milenkovic, C. Lohaus, H.E. Meyer, B. Guiard, C. Meisinger, N. Pfanner, An essential role of Sam50 in the protein sorting and assembly machinery of the mitochondrial outer membrane, J. Biol. Chem. 278 (2003) 48520–48523.
[29] I. Gentle, K. Gabriel, P. Beech, R. Waller, T. Lithgow, The Omp85 family of proteins is essential for outer membrane biogenesis in mitochondria and bacteria, J. Cell Biol. 164 (2004) 19–24.
[30] S.A. Paschen, T. Waizenegger, T. Stan, M. Preuss, M. Cyrklaff, K. Hell, D. Rapaport, W. Neupert, Evolutionary conservation of biogenesis of beta-barrel membrane proteins, Nature 426 (2003) 862–866.

[31] F. Jacob-Dubuisson, V. Villeret, B. Clantin, A.-S. Delattre, N. Saint, First structural insights into the TpsB/Omp85 superfamily, Biol. Chem. 390 (2009) 675–684.
[32] R. Bredemeier, T. Schlegel, F. Ertel, A. Vojta, L. Borissenko, M.T. Bohnsack, M. Groll, A. von Haeseler, E. Schleiff, Functional and phylogenetic properties of the pore-forming beta-barrel transporters of the Omp85 family, J. Biol. Chem. 282 (2007) 1882–1890.
[33] M.T. Bohnsack, E. Schleiff, The evolution of protein targeting and translocation systems, Biochim. Biophys. Acta 1803 (2010) 1115–1130.
[34] E. Schleiff, U.G. Maier, T. Becker, Omp85 in eukaryotic systems: one protein family with distinct functions, Biol. Chem. 392 (2011) 21–27.
[35] B. Clantin, A.S. Delattre, P. Rucktooa, N. Saint, A.C. Meli, C. Locht, F. Jacob-Dubuisson, V. Villeret, Structure of the membrane protein FhaC: a member of the Omp85-TpsB transporter superfamily, Science 317 (2007) 957–961.
[36] N. Noinaj, A.J. Kuszak, J.C. Gumbart, P. Lukacik, H. Chang, N.C. Easley, T. Lithgow, S.K. Buchanan, Structural insight into the biogenesis of β-barrel membrane proteins, Nature 501 (2013) 385–390.
[37] I.R. Boldogh, D.W. Nowakowski, H.-C. Yang, H. Chung, S. Karmon, P. Royes, L.A. Pon, A protein complex containing Mdm10p, Mdm12p, and Mmm1p links mitochondrial membranes and DNA to the cytoskeleton-based segregation machinery, Mol. Biol. Cell 14 (2003) 4618–4627.
[38] C. Meisinger, M. Rissler, A. Chacinska, L.K.S. Szklarz, D. Milenkovic, V. Kozjak, B. Schonfisch, C. Lohaus, H.E. Meyer, M.P. Yaffe, B. Guiard, N. Wiedemann, N. Pfanner, The mitochondrial morphology protein Mdm10 functions in assembly of the preprotein translocase of the outer membrane, Dev. Cell 7 (2004) 61–71.
[39] C. Meisinger, S. Pfannschmidt, M. Rissler, D. Milenkovic, T. Becker, D. Stojanovski, M.J. Youngman, R.E. Jensen, A. Chacinska, B. Guiard, N. Pfanner, N. Wiedemann, The morphology proteins Mdm12/Mmm1 function in the major beta-barrel assembly pathway of mitochondria, EMBO J. 26 (2007) 2229–2239.
[40] B. Kornmann, E. Currie, S.R. Collins, M. Schuldiner, J. Nunnari, J.S. Weissman, P. Walter, An ER-mitochondria tethering complex revealed by a synthetic biology screen, Science 325 (2009) 477–481.
[41] K. Yamano, S. Tanaka-Yamano, T. Endo, Mdm10 as a dynamic constituent of the TOB/SAM complex directs coordinated assembly of Tom40, EMBO Rep. 11 (2010) 187–193.
[42] J.G. Wideman, N.E. Go, A. Klein, E. Redmond, S.W.K. Lackey, T. Tao, H. Kalbacher, D. Rapaport, W. Neupert, F.E. Nargang, Roles of the Mdm10, Tom7, Mdm12, and Mmm1 proteins in the assembly of mitochondrial outer membrane proteins in *Neurospora crassa*, Mol. Biol. Cell 21 (2010) 1725–1736.
[43] N. Thornton, D.A. Stroud, D. Milenkovic, B. Guiard, N. Pfanner, T. Becker, Two modular forms of the mitochondrial sorting and assembly machinery are involved in biogenesis of alpha-helical outer membrane proteins, J. Mol. Biol. 396 (2010) 540–549.
[44] T. Becker, L.-S. Wenz, N. Thornton, D. Stroud, C. Meisinger, N. Wiedemann, N. Pfanner, Biogenesis of mitochondria: dual role of Tom7 in modulating assembly of the preprotein translocase of the outer membrane, J. Mol. Biol. 405 (2011) 113–124.
[45] K. Yamano, S. Tanaka-Yamano, T. Endo, Tom7 regulates Mdm10-mediated assembly of the mitochondrial import channel protein Tom40, J. Biol. Chem. 285 (2010) 41222–41231.
[46] B. Kornmann, C. Osman, P. Walter, The conserved GTPase Gem1 regulates endoplasmic reticulum–mitochondria connections, Proc. Natl. Acad. Sci. U. S. A. 108 (2011) 14151–14156.
[47] D.A. Stroud, S. Oeljeklaus, S. Wiese, M. Bohnert, U. Lewandrowski, A. Sickmann, B. Guiard, M. van der Laan, B. Warscheid, N. Wiedemann, Composition and topology of the endoplasmic reticulum–mitochondria encounter structure, J. Mol. Biol. 413 (2011) 743–750.
[48] C. Voss, B.P. Lahiri, B.P. Young, C.J. Loewen, W.A. Prinz, ER-shaping proteinsfacilitate lipid exchange between the ER and mitochondria in S. cerevisiae, J. Cell Sci. 125 (Pt 20) (2012) 4791–4799.
[49] T. Tan, C. Ozbalci, B. Brugger, D. Rapaport, K.S. Dimmer, Mcp1 and Mcp2, two novel proteins involved in mitochondrial lipid homeostasis, J. Cell Sci. 126 (2013) 3563–3574.
[50] K.O. Kopec, V. Alva, A.N. Lupas, Homology of SMP domains to the TULIP superfamily of lipid-binding proteins provides a structural basis for lipid exchange between ER and mitochondria, Bioinformatics 26 (2010) 1927–1931.
[51] K.O. Kopec, V. Alva, A.N. Lupas, Bioinformatics of the TULIP domain superfamily, Biochem. Soc. Trans. 39 (2011) 1033–1038.
[52] L.F. Sogo, M.P. Yaffe, Regulation of mitochondrial morphology and inheritance by Mdm10p, a protein of the mitochondrial outer membrane, J. Cell Biol. 126 (1994) 1361–1373.
[53] I. Boldogh, N. Vojtov, S. Karmon, L.A. Pon, Interaction between mitochondria and the actin cytoskeleton in budding yeast requires two integral mitochondrial outer membrane proteins, Mmm1p and Mdm10p, J. Cell Biol. 141 (1998) 1371–1381.
[54] L.J. Garcia-Rodriguez, D.G. Crider, A. Gay, I.J. Salanueva, I.R. Boldogh, L.A. Pon, Mitochondrial inheritance is required for MEN-regulated cytokinesis in budding yeast, Curr. Biol. 19 (2009) 1730–1735.
[55] C. Osman, M. Haag, C. Potting, J. Rodenfels, P.V. Dip, F.T. Wieland, B. Brugger, B. Westermann, T. Langer, The genetic interactome of prohibitins: coordinated control of cardiolipin and phosphatidylethanolamine by conserved regulators in mitochondria, J. Cell Biol. 184 (2009) 583–596.
[56] Y. Tamura, O. Onguka, A.E. Hobbs, R.E. Jensen, M. Iijima, S.M. Claypool, H. Sesaki, Role for two conserved intermembrane space proteins, Ups1p and Ups2p, in intra-mitochondrial phospholipid trafficking, J. Biol. Chem. 287 (2012) 15205–15218.
[57] T.T. Nguyen, A. Lewandowska, J.Y. Choi, D.F. Markgraf, M. Junker, M. Bilgin, C.S. Ejsing, D.R. Voelker, T.A. Rapoport, J.M. Shaw, Gem1 and ERMES do not directly affect phosphatidylserine transport from ER to mitochondria or mitochondrial inheritance, Traffic 13 (16) (2012) 880–890.
[58] N. Wiedemann, V. Kozjak, A. Chacinska, B. Schonfisch, S. Rospert, M. Ryan, N. Pfanner, C. Meisinger, Machinery for protein sorting and assembly in the mitochondrial outer membrane, Nature 424 (2003) 565–571.
[59] S. Kutik, D. Stojanovski, L. Becker, T. Becker, M. Meinecke, V. Kruger, C. Prinz, C. Meisinger, B. Guiard, R. Wagner, N. Pfanner, N. Wiedemann, Dissecting membrane insertion of mitochondrial beta-barrel proteins, Cell 132 (2008) 1011–1024.
[60] K. Imai, N. Fujita, M.M. Gromiha, P. Horton, Eukaryote-wide sequence analysis of mitochondrial beta-barrel outer membrane proteins, BMC Genomics 12 (2011) 79.
[61] D. Stojanovski, N. Pfanner, N. Wiedemann, Import of proteins into mitochondria, Methods Cell Biol. 80 (2007) 783–806.
[62] D. Stojanovski, B. Guiard, V. Kozjak-Pavlovic, N. Pfanner, C. Meisinger, Alternative function for the mitochondrial SAM complex in biogenesis of alpha-helical TOM proteins, J. Cell Biol. 179 (2007) 881–893.
[63] M. Bohnert, L.-S. Wenz, R.M. Zerbes, S.E. Horvath, D.A. Stroud, K. von der Malsburg, J.M. Muller, S. Oeljeklaus, I. Perschil, B. Warscheid, A. Chacinska, M. Veenhuis, van der Kleil.J. , G. Daum, N. Wiedemann, T. Becker, N. Pfanner, M. van der Laan, Role of mitochondrial inner membrane organizing system in protein biogenesis of the mitochondrial outer membrane, Mol. Biol. Cell 23 (2012) 3948–3956.
[64] M. Punta, P. Coggill, R. Eberhardt, J. Mistry, J. Tate, C. Boursnell, N. Pang, K. Forslund, G. Ceric, J. Clements, A. Heger, L. Holm, E. Sonnhammer, S. Eddy, A. Bateman, R. Finn, The Pfam protein families database, Nucleic Acids Res. 40 (2012) D290–D301.
[65] W. Li, A. Godzik, Cd-hit: a fast program for clustering and comparing large sets of protein or nucleotide sequences, Bioinformatics 22 (2006) 1658–1659.
[66] K. Katoh, H. Toh, Recent developments in the MAFFT multiple sequence alignment program, Brief. Bioinform. 9 (2008) 286–298.
[67] T. Frickey, A. Lupas, CLANS: a Java application for visualizing protein families based on pairwise similarity, Bioinformatics 20 (2004) 3702–3704.
[68] A. Stamatakis, RAxML-VI-HPC: maximum likelihood-based phylogenetic analyses with thousands of taxa and mixed models, Bioinformatics 22 (2006) 2688–2690.
[69] D. Darriba, G.L. Taboada, R. Doallo, D. Posada, ProtTest 3: fast selection of best-fit models of protein evolution, Bioinformatics 27 (2011) 1164–1165.
[70] A. Stamatakis, P. Hoover, J. Rougemont, A rapid bootstrap algorithm for the RAxML Web servers, Syst. Biol. 57 (2008) 758–771.
[71] A. Stamatakis, Phylogenetic models of rate heterogeneity: A high performance computing perspective, in proceedings of the 20th international parallel and distributed processing symposium (IPDPS), http://citeseerx.ist.psu.edu/viewdoc/summary?doi=10.1.1.79.15462006.
[72] N. Lartillot, T. Lepage, S. Blanquart, PhyloBayes 3: a Bayesian software package for phylogenetic reconstruction and molecular dating, Bioinformatics 25 (2009) 2286–2288.
[73] S.F. Altschul, T.L. Madden, A.A. Schaffer, J. Zhang, Z. Zhang, W. Miller, D.J. Lipman, Gapped BLAST and PSI-BLAST: a new generation of protein database search programs, Nucleic Acids Res. 25 (1997) 3389–3402.
[74] S. Henikoff, J.G. Henikoff, Amino acid substitution matrices from protein blocks, Proc. Natl. Acad. Sci. U. S. A. 89 (1992) 10915–10919.
[75] N. Eswar, B. Webb, M.A. Marti-Renom, M.S. Madhusudhan, D. Eramian, M.-Y. Shen, U. Pieper, A. Sali, Comparative protein structure modeling using Modeller, Curr. Protoc. Bioinform. 5 (2006)(Unit 5.6).
[76] E. Krieger, T. Darden, S.B. Nabuurs, A. Finkelstein, G. Vriend, Making optimal use of empirical energy functions: force-field parameterization in crystal space, Proteins 57 (2004) 678–683.
[77] J. Soding, Protein homology detection by HMM–HMM comparison, Bioinformatics 21 (2005) 951–960.
[78] L. Jaroszewski, L. Rychlewski, Z. Li, W. Li, A. Godzik, FFAS03: a server for profile–profile sequence alignments, Nucleic Acids Res. 33 (2005) W284–W288.
[79] L.A. Kelley, M.J.E. Sternberg, Protein structure prediction on the Web: a case study using the Phyre server, Nat. Protoc. 4 (2009) 363–371.
[80] N. Flinner, E. Schleiff, O. Mirus, Identification of two voltage-dependent anion channel-like protein sequences conserved in Kinetoplastida, Biol. Lett. 8 (3) (2012) 446–449.
[81] E.W. Dijkstra, A note on two problems in connexion with graphs, Numer. Math. 1 (1959) 269–271(http://www-m3.ma.tum.de/twiki/pub/MN0506/WebHome/dijkstra.pdf).
[82] A.G. Murzin, S.E. Brenner, T. Hubbard, C. Chothia, SCOP: a structural classification of proteins database for the investigation of sequences and structures, J. Mol. Biol. 247 (1995) 536–540.
[83] J.-M. Chandonia, G. Hon, N.S. Walker, L. Lo Conte, P. Koehl, M. Levitt, S.E. Brenner, The ASTRAL compendium in 2004, Nucleic Acids Res. 32 (2004) D189–D192.
[84] B. van den Berg, P.N. Black, W.M. Clemons Jr., T.A. Rapoport, Crystal structure of the long-chain fatty acid transporter FadL, Science 304 (2004) 1506–1509.
[85] S. Krieg, F. Huche, K. Diederichs, N. Izadi-Pruneyre, A. Lecroisey, C. Wandersman, P. Delepelaire, W. Welte, Heme uptake across the outer membrane as revealed by crystal structures of the receptor–hemophore complex, Proc. Natl. Acad. Sci. U. S. A. 106 (2009) 1045–1050.
[86] M.A. Kurowski, J.M. Bujnicki, GeneSilico protein structure prediction meta-server, Nucleic Acids Res. 31 (2003) 3305–3307.
[87] C. Schaefer, A. Schlessinger, B. Rost, Protein secondary structure appears to be robust under in silico evolution while protein disorder appears not to be, Bioinformatics 26 (2010) 625–631.
[88] A.K. Dunker, M.S. Cortese, P. Romero, L.M. Iakoucheva, V.N. Uversky, Flexible nets. The roles of intrinsic disorder in protein interaction networks, FEBS J. 272 (2005) 5129–5148.
[89] Z. Dosztanyi, J. Chen, A.K. Dunker, I. Simon, P. Tompa, Disorder and sequence repeats in hub proteins and their implications for network evolution, J. Proteome Res. 5 (2006) 2985–2995.

[90] J. Gsponer, M.M. Babu, The rules of disorder or why disorder rules, Prog. Biophys. Mol. Biol. 99 (2–3) (2009) 94–103.
[91] C.J. Oldfield, J. Meng, J.Y. Yang, M.Q. Yang, V.N. Uversky, A.K. Dunker, Flexible nets: disorder and induced fit in the associations of p53 and 14-3-3 with their partners, BMC Genomics 9 (Suppl. 1) (2008) S1.
[92] K.S. Dimmer, S. Fritz, F. Fuchs, M. Messerschmitt, N. Weinbach, W. Neupert, B. Westermann, Genetic basis of mitochondrial function and morphology in *Saccharomyces cerevisiae*, Mol. Biol. Cell 13 (2002) 847–853.
[93] C. Meisinger, N. Wiedemann, M. Rissler, A. Strub, D. Milenkovic, B. Schonfisch, H. Muller, V. Kozjak, N. Pfanner, Mitochondrial protein sorting: differentiation of beta-barrel assembly by Tom7-mediated segregation of Mdm10, J. Biol. Chem. 281 (2006) 22819–22826.
[94] M. Guharoy, P. Chakrabarti, Conserved residue clusters at protein–protein interfaces and their use in binding site identification, BMC Bioinform. 11 (2010) 286.
[95] M. Remmert, A. Biegert, D. Linke, A.N. Lupas, J. Soding, Evolution of outer membrane β-barrels from an ancestral ββ hairpin, Mol. Biol. Evol. 27 (2010) 1348–1358.
[96] R. Derelle, B.F. Lang, Rooting the eukaryotic tree with mitochondrial and bacterial proteins, Mol. Biol. Evol. 29 (2012) 1277–1289.
[97] D. Milenkovic, V. Kozjak, N. Wiedemann, C. Lohaus, H.E. Meyer, B. Guiard, N. Pfanner, C. Meisinger, Sam35 of the mitochondrial protein sorting and assembly machinery is a peripheral outer membrane protein essential for cell viability, J. Biol. Chem. 279 (2004) 22781–22785.
[98] N.C. Chan, T. Lithgow, The peripheral membrane subunits of the SAM complex function codependently in mitochondrial outer membrane biogenesis, Mol. Biol. Cell 19 (2008) 126–136.
[99] T. Waizenegger, S.J. Habib, M. Lech, D. Mokranjac, S.A. Paschen, K. Hell, W. Neupert, D. Rapaport, Tob38, a novel essential component in the biogenesis of beta-barrel proteins of mitochondria, EMBO Rep. 5 (2004) 704–709.
[100] D. Ishikawa, H. Yamamoto, Y. Tamura, K. Moritoh, T. Endo, Two novel proteins in the mitochondrial outer membrane mediate beta-barrel protein assembly, J. Cell Biol. 166 (2004) 621–627.
[101] L. Delage, C. Leblanc, P. Nyvall Collen, B. Gschloessl, M.-P. Oudot, L. Sterck, J. Poulain, J.-M. Aury, J.M. Cock, In silico survey of the mitochondrial protein uptake and maturation systems in the brown alga *Ectocarpus siliculosus*, PLoS One 6 (2011) e19540.
[102] A. Murley, L.L. Lackner, C. Osman, M. West, G.K. Voeltz, P. Walter, J. Nunnari, ER-associated mitochondrial division links the distribution of mitochondria and mitochondrial DNA in yeast, eLife 2 (2013) e00422.
[103] L.A. Staehelin, The plant ER: a dynamic organelle composed of a large number of discrete functional domains, Plant J. 11 (1997) 1151–1165.
[104] O.M. de Brito, L. Scorrano, Mitofusin 2 tethers endoplasmic reticulum to mitochondria, Nature 456 (2008) 605–610.
[105] G. Szabadkai, K. Bianchi, P. Varnai, S.D. De, M.R. Wieckowski, D. Cavagna, A. Nagy, T. Balla, R. Rizzuto, Chaperone-mediated coupling of endoplasmic reticulum and mitochondrial Ca^{2+} channels, J. Cell Biol. 175 (2006) 901–911.
[106] R. Iwasawa, A.-L. Mahul-Mellier, C. Datler, E. Pazarentzos, S. Grimm, Fis1 and Bap31 bridge the mitochondria-ER interface to establish a platform for apoptosis induction, EMBO J. 30 (2011) 556–568.
[107] D. Price, C. Chan, H. Yoon, E. Yang, H. Qiu, A.P.M. Weber, R. Schwacke, J. Gross, N.A. Blouin, C. Lane, A. Reyes-Prieto, D.G. Durnford, J.A.D. Neilson, B.F. Lang, G. Burger, J.M. Steiner, W. Loffelhardt, J.E. Meuser, M.C. Posewitz, S. Ball, M.C. Arias, B. Henrissat, P.M. Coutinho, S.A. Rensing, A. Symeonidi, H. Doddapaneni, B.R. Green, V.D. Rajah, J. Boore, D. Bhattacharya, *Cyanophora paradoxa* genome elucidates origin of photosynthesis in algae and plants, Science 335 (2012) 843–847.
[108] Z. Dosztanyi, V. Csizmok, P. Tompa, I. Simon, The pairwise energy content estimated from amino acid composition discriminates between folded and intrinsically unstructured proteins, J. Mol. Biol. 347 (2005) 827–839.
[109] J. Kyte, R.F. Doolittle, A simple method for displaying the hydropathic character of a protein, J. Mol. Biol. 157 (1982) 105–132.
[110] K. Tamura, D. Peterson, N. Peterson, G. Stecher, M. Nei, S. Kumar, MEGA5: molecular evolutionary genetics analysis using maximum likelihood, evolutionary distance, and maximum parsimony methods, Mol. Biol. Evol. 28 (2011) 2731–2739.
[111] K. Shalchian-Tabrizi, M.A. Minge, M. Espelund, R. Orr, T. Ruden, K.S. Jakobsen, T. Cavalier-Smith, Multigene phylogeny of choanozoa and the origin of animals, PLoS One 3 (2008) e2098.
[112] T. Cavalier-Smith, Kingdoms Protozoa and Chromista and the eozoan root of the eukaryotic tree, Biol. Lett. 6 (2010) 342–345.